Faraday Discussions

Accepted Manuscript

This manuscript will be presented and discussed at a forthcoming Faraday Discussion meeting. All delegates can contribute to the discussion which will be included in the final volume.

Register now to attend! Full details of all upcoming meetings: http://rsc.li/fd-upcoming-meetings

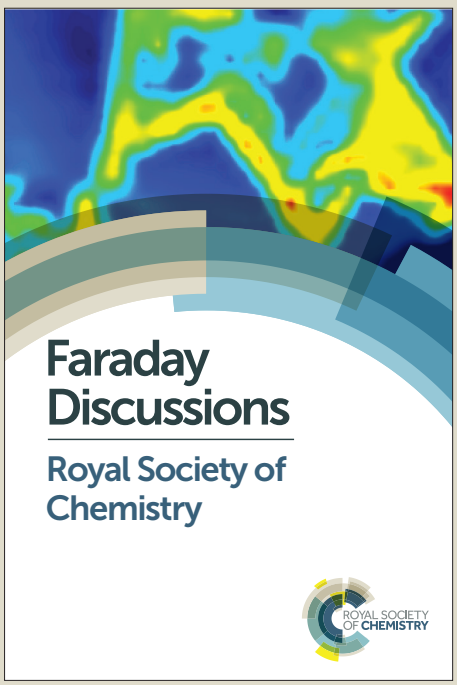

This is an *Accepted Manuscript*, which has been through the Royal Society of Chemistry peer review process and has been accepted for publication.

Accepted Manuscripts are published online shortly after acceptance, before technical editing, formatting and proof reading. Using this free service, authors can make their results available to the community, in citable form, before we publish the edited article. We will replace this *Accepted Manuscript* with the edited and formatted *Advance Article* as soon as it is available.

You can find more information about *Accepted Manuscripts* in the Information for Authors.

Please note that technical editing may introduce minor changes to the text and/or graphics, which may alter content. The journal's standard Terms & Conditions and the Ethical guidelines still apply. In no event shall the Royal Society of Chemistry be held responsible for any errors or omissions in this *Accepted Manuscript* or any consequences arising from the use of any information it contains.

ROYAL SOCIETY OF CHEMISTRY

www.rsc.org/faraday_d

Journal Name

ARTICLE

Colloidal Assembly by Ice Templating

Guruswamy Kumaraswamy,[a*] Bipul Biswas[a] and Chandan K. Choudhury[a]

Received 00th January 20xx,
Accepted 00th January 20xx

DOI: 10.1039/x0xx00000x

www.rsc.org/

We investigate ice templating of aqueous dispersions of polymer coated colloids and crosslinker, at particle concentrations far below that required to form percolated monoliths. Freezing the aqueous dispersions forces particles into close proximity to form clusters, that are held together as polymer chains coating the particles are crosslinked. We observe that, with increase in particle concentration from about 10^6 to 10^8 particles/ml, there is a transition from isolated single particles to increasingly larger clusters. In this concentration range, most of the colloidal clusters formed are linear or sheet like particle aggregates. Remarkably, the cluster size distribution for clusters smaller than about 30 particles, as well as the size distribution of linear clusters, is only weakly dependent on the dispersion concentration in the range that we investigate. We demonstrate that the main features of cluster formation are captured by kinetic simulations that do not consider hydrodynamics or instabilities at the growing ice front due to particle concentration gradients. Thus, clustering of colloidal particles by ice templating dilute dispersions appears to be governed only by particle exclusion by the growing ice crystals that leads to their accumulation at ice crystal boundaries.

Introduction

When an aqueous solution or dispersion is frozen, the ice crystals that form, exclude solutes and dispersed particles. These solutes or dispersed particles are spatially localized in the interstitial regions between ice crystals that form as water freezes. Subsequent removal of the ice, typically by freeze drying, results in formation of a porous material as a negative replica of the ice crystals. This process, called ice templating or ice segregation-induced self-assembly (ISISA) has emerged as a powerful technique for the production of macroporous materials.[1-3] There are several advantages to ice templating: it uses water as a solvent and is therefore, environmentally friendly and economical. Further, the processing equipment required to practise ice templating are widely accessible since they are relatively inexpensive.

Ice templating is not a new technique: reports of usage of synthetic cryogels in the biomedical literature go back several decades.[4-5] Ice templating has been used to prepare porous monoliths from rubber latex,[6] from thermoset resorcinol-formaldehyde,[7] as well as from a wide variety of biocompatible polymers, including, collagen, polylactic acid, polyglycolic acid, gelatin, etc.[8-12] Freeze-drying induced partial crystallization of polymers, such as poly(vinyl alcohol) has also been used to generate porous structures.[13] Ice templating of ceramic slurries has been employed to freeze cast a variety of near net shape porous products. Recently, there has been tremendous interest in combining ice templating with directional freezing to produce oriented structures. This was pioneered by researchers from DuPont[14] who demonstrated that directional freezing of an aqueous solution of silicic acid and its subsequent polymerization resulted in the formation of oriented silica wires. In the last decade, researchers have extended directional ice templating to produce aligned titania fibers[15] and macroporous aligned honeycomb monoliths of silica or combinations of alumina and silica.[16,17] Aligned 1-D and 2-D structures comprising of polymer or polymer-inorganic composites have also been produced by directional templating followed by freeze drying.[18] Nacre-like tough layered composites have been produced in a two-step process by forming alumina sheets through directional ice templating, followed by in-filling with either epoxy or metal[19-20] or even a glassy phase.[21] Oriented anisotropic polymer nanocomposite hybrids have also been reported by other researchers,[22-24] attesting to the versatility of directional ice templating.

Control over the properties of ice-templated materials requires a thorough understanding of the development of structure as solutes or dispersed particles are organized by growing ice crystals. Apart from porous materials synthesis, this understanding has implications for waste water treatment[25] and geophysical phenomena such as freezing of wet soil.[26] The interaction between dispersed particles and a solid-liquid interface was examined by Uhlmann and co-workers.[27] By balancing the hydrodynamic lubrication forces experienced by a suspended particle as it is approached by a growing solid interface, with the attractive interaction between the particle and the interface, they determined a critical velocity for the interface, above which the particles are

[a] Complex Fluids and Polymer Engineering, Polymer Science and Engineering Division, CSIR-National Chemical Laboratory, Dr. Homi Bhabha Road, Pune 411008, India.
Correspondence to: Guruswamy Kumaraswamy, g.kumaraswamy@ncl.res.in, Tel: +91-20-2590-2182, Fax: +91-20-2590-2618

overgrown by the solid medium and trapped within it. At velocities lower than the critical velocity, particles are unable to penetrate the growing solid front and are aggregated at the liquid-solid interface. Experimental studies[28] suggested that this critical velocity for particle trapping as water was frozen, was higher in ice grain boundary grooves. The presence of a gradient of temperature or solute concentration at the ice-water interface can also influence ice growth. The ice front can become unstable as a consequence of such gradients and break up into cellular structures, characterized by a wavelength, $\mathbf{l}_c$, that is predicted by the linear Mullins-Sekerka theory.[29-31] The presence of particles at the ice growth front also results in constitutional undercooling and depresses the freezing point of the water – similar to the case of atomic or molecular systems. Further, as particles accumulate at the ice front, the transport properties change in a highly nonlinear manner – unlike the case of atomic or molecular systems. By carefully accounting for these, significant progress has recently been made in understanding ice structure formation during freezing of aqueous colloidal dispersions and theoretical estimates of the conditions for the onset of growth instabilities are now available.[32-33] Following this approach, the group of Deville[34-37] has determined an experimental phase diagram for instabilities in ice growth in colloidal dispersions. Specifically, they have identified regions where particles are rejected by the ice and are concentrated at the ice-water interface, as well as metastable and unstable regions, where transverse ice lenses are likely to form. We note that, based on their observations, particles up to a micron in size are always rejected by the growing ice front for ice growth velocities of ~O(0.1 – 1 μm/s).

Thus, while experimental implementation of ice templating is simple, a detailed understanding of the effects of solute and colloids on solidification is important for controlling the structure of the porous aggregate formed. Our understanding of structure development during freezing of aqueous systems containing both dispersed colloid and dissolved polymers is incomplete. For example, Zhang and co-workers[18] note that the presence of a small fraction of polymer, poly (vinyl alcohol) critically influences the shape of the ice-templated structures formed by directional ice-templating of silica colloidal dispersions. Plate like objects are formed in the absence of the polymer while aligned porous structures resulted while ice-templating polymer/colloid hybrids. Similarly, Shi and co-workers[22] have noted that the presence of a polymeric "mortar" (in their case, poly-N-isopropylacrylamide) was essential for the formation of anisotropic rod morphologies by direction ice templating of silica particle dispersions. The reasons that underly these observations are not fully understood at this time.

Recently, we have demonstrated[38] the formation of porous hybrid structures by ice templating an aqueous dispersion containing rigid colloidal particles, polymer and crosslinker, followed by crosslinking of the hybrid structure in the frozen state. This process does not require freeze drying since the hybrid structure is covalently crosslinked. Thus, the ice can simply be thawed to recover a porous monolith. Remarkably, we observe that these monoliths are elastic and can be reversibly compressed to about 10% of their original size – even when the inorganic content exceeds 90% by weight. This behaviour was observed for porous materials prepared using various colloids (silica particles, polystyrene latex and hydroxyapatite particles), for different polymers (polyethyleneimine and gelatin) and for different crosslinking chemistries. We concluded that the mechanical response observed was a consequence of a unique microstructure in the particle-polymer hybrid that was created by crosslinking during ice templating.

In most of the previous investigations, the focus was on the synthesis of macroscopic assemblies or monoliths. Therefore, these studies used colloidal dispersions containing a relatively large volume fraction of colloids. In this work, we investigate the formation of colloidal aggregates by ice templating extremely dilute colloidal dispersions and by crosslinking the assemblies of polymer coated colloids in the frozen state. The dispersion concentrations used here are far below that required for a transition to percolated porous monoliths. We demonstrate that the colloidal assemblies exhibit a progression of shapes from linear assemblies to tape-like structures to 2D aggregates. Simulations that rely on a simple kinetic model of particles being expelled by growing ice crystals are able to capture the qualitative features of the particle clusters formed.

Materials and Methods

Materials

Poly(ethylene imine), PEI (50% w/v solution; molecular weight specified by supplier, M_w = 750 kg/mol) and; polyethyleneglycol diepoxide (PEG-diepoxide, supplier specified M_n = 500 g/mol) were obtained from Sigma-Aldrich and were used as received. Fluorescent polystyrene (PS) latex particles, 1.04 μm in size with a polydispersity of 4% were used as received from Microparticle GmbH, Germany. These particles were negatively charged with sulphonic acid groups on their surface and were supplied as 2.5% w/v aqueous dispersions. DI water was used from a Millipore system (pH = 7, resistivity = 18.2 MΩcm).

Sample Preparation

1μL of PS latex dispersion (containing ≈ 2.96×10^8 colloidal particles) was added to 100 μL DI water. This was sonicated for one minute, followed by a minute of vortexing to prepare a uniform colloidal dispersion. 1.5μL of a stock solution of PEI (prepared by adding 100 mg of as received PEI in 1ml of DI water) was diluted by adding to 100μL DI water and vortexing for 2 minutes. While the PEI solution is vortexed, the latex dispersion is added slowly. After addition of the latex, the sample is centrifuged at 3000 rpm for 8 minutes. The supernatant (corresponding to about 75% of the solution) is

carefully removed using a micropipette. We note that there is almost no loss of particles in the washing step since only about 75% of the supernatant is removed and since care is taken to pipette it out gently. 200µL DI water is added to the sedimented latex particles and they were redispersed by ultrasonication for two minutes and vortexing for one minute. Subsequently, the dispersion is further diluted by addition of 280µL DI water. This washing step, viz. centrifugation and redispersion was performed one more time. 3µL PEG-diepoxide is diluted in 100µL of water and vortexed for a minute. To this, the latex dispersion is added while continuously vortexing. After addition of the latex dispersion, the sample is transferred to a freezer maintained at -18°C and is stored for 12 hours, during which time the water freezes, and crosslinking proceeds. A schematic of the ice-templating process is shown in Figure 1. Subsequently, the sample is thawed at room temperature for 30-40 minutes and is loaded in a microscope cavity slide and sealed. Particles and particle clusters in the sealed sample are allowed to settle over an hour before the sample is imaged. Similarly, we prepare samples at different particle concentrations: 5.41 x 10^7 particles/ml, 7.39 x 10^7 particles/ml, 3.39 x 10^6 particles/ml and 8.46 x 10^5 particles/ml.

Experimental Methods and Data Analysis

Laser Scanning Fluorescence Microscopy was performed using a Carl Zeiss Axio Observer with, a 40X objective (NA = 0.75 and working distance = 0.71 mm). Laser light (wavelength = 543 nm) was used to excite the fluorescent PS particles and images were collected using a 610 nm emission filter. We collected over 200 images at each concentration and analysed these to characterize particle clustering. At the lowest particle concentration (8.46 x 10^5 particles/ml), images containing nearly 7500 were analysed while at the highest concentration (2.96 × 10^8 particles/ml), there were nearly 140,000 particles in the images analysed.

Image analysis was performed using Image J software. After subtraction of a constant background, the images were thresholded and converted into binary. We then employed the inbuilt particle analysis option in Image J to obtain the area and perimeter of each cluster in the image.

Computational Details

In our simulation scheme to investigate aggregate formation during ice templating, we use Brownian dynamics to model the motion of individual colloids. We anticipate, based on our experiments, that colloid aggregation is essentially a kinetic phenomenon, driven by particle expulsion at the water-ice interface. Thus, we implement a minimal simulation scheme, where we neglect hydrodynamic interactions between colloids. Colloidal particles are modelled as hard spheres, with a diffusion coefficient (D = 0.2235 µm^{2}s^{-1}) that is estimated from the Stokes Einstein relation for 1 µm colloids diffusing in water at a temperature, T = 273.15K. Thus,

$$D = (k_B\, T)/(6\, \pi\, \eta\, a) \qquad (1)$$

where, k_B is the Boltzmann constant, η is the viscosity of water at 273.15 K, and a (= 0.5 µm) is the radius of the colloidal particles.

We implement our simulation by updating the position of particles (x) as in Equation 2.

$$x = x + \sqrt{2Ddt}\; r \qquad (2)$$

where r is a random number drawn from a normal distribution with mean = 0 and standard deviation = 1 and dt represents the simulation time step. The time step was set to 0.5 ms. The size of the colloidal particles was taken as unity. We allow the colloidal particles to translate in three dimensions according to Equation 2. We carried out simulations for dilute dispersions of the colloidal particles, in the absence of ice crystals and confirmed that the mean square displacement is linear in time and has a diffusion constant (obtained from the slope) of 0.22 µm^{2}s^{-1}.

We start ice templating simulations by placing colloidal particles and ice nuclei, with their centers randomly located in the simulation box. At the start of the simulation, ice nuclei were treated as point particles with a size of 10^{-3} times that of the colloidal particles. In our scheme, all the ice crystals nucleate at t = 0 and grow isotropically with a growth rate of 100 nm s^{-1} (viz. 0.1 units/s). The value of the growth rate is based on experimental estimates for ice growth in our experiments (see Results section). The number density of ice nuclei is chosen to correspond with the average number density of ice crystals in our experiments.

As the ice crystals grow, the motion of the colloidal particles is restricted since the volume available to the particles decreases. We implement the following rules to dictate particle motion:

(a) If a particle overlaps with another particle during a move, then the move is rejected.

(b) If a particle overlaps with an ice crystal, the motion is reflected. Thus, if a move: $x_p = x_p + \delta x$, results in overlap of the particle position with ice, then we implement: $x_p = x_p - \delta x$ (where $\boldsymbol{x_p}$ is the position of the colloid and $|\delta \boldsymbol{x}|$ =$\sqrt{2Ddt}\; r$, is its translation, determined by Equation 2). If the particle overlaps with an ice particle even after the move is mirrored, the move is rejected. Initially all systems were equilibrated for 2500 steps. These equilibrated coordinates were used to investigate the effect of ice growth on the aggregation of colloidal particles. The simulations were stopped when we visually observed aggregation of the colloidal particles, resulting in a cessation of their Brownian motion. The trajectory was written after every 500 ms (= 1000 steps). Aggregation time was observed to vary with particle concentration. All simulations were carried out in triplicate, using three sets of initial coordinates.

We investigated systems with particle concentrations of 10^6, 10^7, 10^8, and 10^9 colloidal particles per ml. The number of particles, ice nuclei and box dimensions corresponding to these concentrations are tabulated in Table 1. We employed

periodic boundary conditions in all three directions and used minimum image convention.[39]

Results and Discussion

The PS colloids used in these experiments are negatively charged and therefore, PEI chains adsorb on their surface. We have previously characterized the adsorption of PEI on these latices using zeta potential measurements.[40] In this work, a dilute aqueous dispersion of PEI coated PS colloids is frozen, by storing at -18°C. As the water forms ice crystals, particles, PEI and crosslinker are expelled at the water-ice boundary. Recently, we have reported[38] the preparation of macroporous colloid/crosslinked PEI hybrid materials by ice-templating of particle dispersions (at particle concentrations that are significantly higher than in this work). These macroporous monoliths were characterized by approximately isotropic pores. Also, while the pores were not monodisperse, most pores were within a factor of 1.5 from the mean size. As the pores are templated by ice crystals, these observations suggest that our freezing protocol results in the formation of ice crystals that are approximately uniform in size and that are nucleated in a spatially random manner. We anticipate that this will also hold for ice crystals in the experiments reported here. In accordance with this expectation, optical microscopy on thin (~50 – 100 μm) samples of dilute latex dispersions, frozen in a cold stage, showed the formation of randomly nucleated ice crystals that had a monomodal size distribution. We can estimate the average growth rate of ice crystals from the time for the sample to freeze, assuming that the ice crystals formed are uniform. This gives a growth rate ~O(0.1 μm/s). Microscopic observations also indicate that the colloidal particles are accumulated at the growing ice-water front. This is consistent with recent calculations[33] and with reported experimental "phase diagram".[34] As the water freezes, both the PEI coated colloids and the diepoxide crosslinker are concentrated at the boundaries of the ice crystals. We use an excess of diepoxide crosslinker to ensure that PEI coated particles that are in contact, are covalently crosslinked. Covalent crosslinking of the PEI proceeds in the frozen state, resulting in the formation of a polymeric mesh around the particles.[38] Thus, colloids that are forced into proximity by the ice crystals form bound aggregates, connected by a crosslinked PEI shell. We allow crosslinking to proceed for 12 hours and subsequently, the sample is thawed. Samples are imaged using a fluorescence microscope to quantify cluster formation.

At the lowest particle concentration (8.46 x 10^5 particles/ml), we observe a large number of "monomers", viz. isolated particles and dimers as well as a few short (~ 4 to 5 particle long) linear strands and planar aggregates (Figure 2, top row). As the concentration increases to 1.35 x 10^7 particles/ml (Figure 2, middle row) and to the highest concentration investigated here, 2.96 x 10^8 particles/ml, we observe the formation of longer linear strands, going up to over 40 particles long, as well as, elongated planar structures that are 2 particles wide (that we term "tapes") and larger planar structures. Interestingly, for the planar structures, we observe that the monodispersity of the colloids drives the formation of locally crystalline structures. Crystalline order has been observed when monodisperse colloidal dispersions undergo gravity-induced sedimentation characterized by small Peclet number ~O(0.1).[41-42] We estimate the Peclet number (Pe) in our experiments based on the growth rate of ice crystals, v. Thus, Pe = vR/D = 0.23, where R is the colloid size and D is the diffusion coefficient of the colloids, consistent with the observation of colloidal crystals. At all concentrations, we observe the formation of only a small fraction of three dimensional aggregates. The majority of the clusters are organized into planar assemblies.

The fraction of particles that form monomers or dimers, $f_n(n < 3)$, is about 0.4 for the lowest concentration (8.46 x 10^5 particles/ml) and this decreases approximately logarithmically with concentration to about 0.15 at 2.96 x 10^8 particles/ml (Figure 3). We term particle aggregates that comprise n≥3 particles as clusters and analyse the cluster size distribution as a function of the particle concentration in the ice-templated aqueous dispersions. We define P_n as the number fraction of clusters comprising n particles. We observe that at the lowest concentration, ice templating does not result in the formation of clusters larger than about 15 particles (Figure 4). However, with increase in concentration, a few clusters larger than 100 particles are observed to form. We note that all the experiments reported here are at concentrations that are significantly below that required for the particles to organize into a percolated network. We observe that, for all the particle concentrations investigated, $P_n \sim n^{-2}$, for clusters comprising $\approx$ n < 30 particles (Figure 4). For larger n, P_n deviates from n^{-2} to exhibit a tail that stretches to increasingly higher n with increase in particle concentration (Figure 4).

Cluster size distributions have been reported to follow a power law in several aggregation processes. When large clusters form by diffusion limited aggregation of clusters, the time dependent cluster size distribution has been observed[43] to follow, $P_n \sim t^{-w} n^{\tau} f(n/t^z)$, where t is the aggregation time and f is a function that asymptotes to 1 at long times. In such diffusion limited cluster aggregation, the power law exponent, $\tau \approx -0.75$. MD simulations of clustering of Lennard-Jones fluids below the percolation threshold has been reported[44] to give $P_n \sim n^{-2.1\pm0.1}$. For fluids with short range attractive and long range repulsive interactions, the cluster size distribution has been shown[45] to follow a power law distribution similar to that for random percolation, viz. $P_n \sim n^{-2.2}$. Glotzer[46] has reported that the distribution of non-percolated clusters of mobile particles as a glass forming Lennard-Jones fluid is cooled scales as $P_n \sim n^{-1.9}$. A similar power law exponent ($P_n \sim n^{-1.7}$) has been reported[47] for distribution of crystalline clusters formed in a concentrated dispersion of monodisperse hard spheres. Thus, cluster size distributions that follow a power law, with a power law exponent close to -2 have been observed for a wide variety of particle aggregation processes. It is interesting that a similar behaviour is observed when particles aggregate during ice templating, and that this scaling

is independent of concentration over a wide concentration range.

Of particular interest are clusters that are organized as connected linear strings of colloidal particles. Such systems represent colloidal analogues of linear polymers and represent promising models for studying fundamental problems in polymer physics. Therefore, there has been significant interest in realizing such linear architectures.[48-60] We plot the number fraction of linear chains as a function of their size (P_n^l = number of linear chains of size n/ total number of linear chains). We observe that 99% of the linear chains have a chain length less than 20 and that the number fraction of linear chains decreases to less than 10^{-3} as n approaches 40 (Figure 5). Remarkably, P_n^l, does not appear to be a very strong function of the colloid concentration in the range of 3.39×10^6 to 2.96×10^8 particles/ml.

Finally, we examine the effect of particle concentration on the shape of the colloidal clusters, focusing on planar assemblies that comprise the majority of the clusters formed. We define a connectivity parameter for a cluster, C as the ratio of the cluster area to the square of the perimeter, viz. C = Area/(Perimeter)^2. An increase in C represents a transition in cluster shape from a linear aggregate towards a circular shape. We calculate the average C at each cluster size, n, for ice templated clusters at various dispersion concentrations (Figure 6). It is difficult to attribute much significance to the variation in C with n. For example, it is easy to visualize that the difference in C between a linear chain and an isotropic planar cluster is small for n = 5, relative to that for larger n, say, n = 50. However, at a fixed cluster size, n, it is possible to comment on the relative values of C for clusters prepared starting from different particle concentrations. We note that there is a systematic increase in C with particle concentration for n > 10 (Figure 6). This indicates that with increase in concentration from 1.35×10^7 to 7.39×10^7 to 2.96×10^8 particles/ml, there is a transition from linear chains to tapes to planar clusters.

Finally, we note that we obtain qualitatively similar data for the cluster size distribution and the evolution of cluster shape when a dispersion of 1μm silica particles are ice-templated using the same experimental protocol. As the specific gravity for the silica particles (≈ 2) is significantly higher than that for the polystyrene latex (≈ 1.05), this indicates that gravitational settling during the freezing process is unimportant in these experiments.

We employ simulations to obtain insights into the mechanism of cluster formation in our experiments. Our simulations incorporate several severe assumptions. Firstly, we completely neglect hydrodynamics in modelling the particle motions. Particles are modelled as hard sphere Brownian colloids with no hydrodynamic interactions. We also assume that all ice crystals are nucleated at the initial time, that their nuclei are fixed in space and that the ice grows as isotropic, spherical crystals until they spatially overlap. Further, we assume that, at the low dispersion concentrations employed in our experiments, growth instabilities of the propagating ice front can be ignored. Finally, we assume that the particles experience repulsion when they encounter the growing ice crystals. The simulation is terminated when particles are confined at ice crystal boundaries and when their motions cease. These assumptions are premised on our intuition that particle aggregation during ice templating of such dilute colloidal dispersions is essentially a kinetic phenomenon. Thus, our simulations model a situation where the only physics that governs particle clustering is their exclusion from growing isotropic ice crystals that are randomly nucleated in space. We anticipate that the results of these simulations are sensitive to the nucleation density and growth rate of ice crystals and use simulation values for these parameters that are based on estimates from our experimental observations.

We present snapshots from the late stages of our simulations, where particle motion has ceased due to the particles being trapped between ice crystals (Figure 7). The ice crystals are not shown in these images, so that the particle clusters can be easily visualized. At low particle concentration (10^6 particles/ml), we observe that most colloids exist as isolated monomeric objects. With increase in particle concentration, we see the emergence of small particle clusters (at 10^7 particles/ml) that transition to larger clusters (at 10^8 particles/ml) and finally, we observe the formation of several three dimensional structures at 10^9 particles/ml (Figure 7). Visually, we observe a transition from isolated colloids to short linear structures to more isotropic planar aggregates and finally to large three-dimensional clusters with increase in particle concentration, in qualitative accord with our experimental observations. As in our experiments, we observe local crystalline ordering in the planar aggregates and three dimensional clusters (Figure 7, right). The number of particles that exist as monomers and dimers decreases, approximately logarithmically, with the dispersion concentration (Supporting information, Figure S1), in qualitative accord with our experimental results (Figure 3). However, the agreement with experiments is not quantitative, probably due to the large number of simplifying assumptions in our simulations.

We obtain a cluster size distribution (P_n) for ice template aggregates as a function of dispersion concentration. Our simulations sample a smaller number of clusters relative to our experiments. Therefore, while we observe the formation of a very small fraction of large colloidal aggregates in our experiments (Figure 4), these are not observed in our simulations. Remarkably, our simulations show that for small n ($< \approx 20$), $P_n \sim n^{-2}$, independent of ice-templated dispersion concentration from 10^7 to 10^9 particles/ml (Figure 8). Beyond this power law region, there is a dispersion concentration-dependent deviation in P_n. The similarity in the trends in P_n obtained from simulations with those from experiments is striking. Similarly, the size distribution of linear colloidal chains, P_n^l obtained from the simulations is independent of dispersion concentration between 10^6 and 10^9 particles/ml (Figure 9), in qualitative accord with our experimental data (compare with Figure 5).

Therefore, despite the numerous simplifying assumptions, our simulations are able to accurately capture qualitative

trends in the size and shape distribution of particle clusters formed during ice templating. This suggests that, at low concentrations, particle clustering during ice templating is purely kinetic in origin.

Conclusions

Ice templating very dilute colloidal dispersions (containing ≈ 10^6 to ≈ 10^8 particles/ml) results in the formation of clusters. With increase in particle concentration in the ice templated dispersion, the average cluster size increases and there is a transition from linear clusters to two-particle wide "tapes" to more isotropic two-dimensional shapes. We observe relatively few large three-dimensional clusters in this range of particle concentration. In this concentration range, the cluster size distribution exhibits a power law, $P_n \sim n^{-2}$, for clusters containing less than ≈ 30 particles, independent of the dispersion concentration. The distribution of linear colloidal clusters is also only weakly dependent on dispersion concentration. Simulations that ignore hydrodynamic interactions between colloidal particles and that model exclusion of particles by randomly nucleated, isotropically growing ice crystals capture the essential features of our experimental observations. This suggests that, for low colloidal concentrations, clustering during ice templating is purely kinetic in origin.

Acknowledgements

We acknowledge funding from the Science and Engineering Research Board, Department of Science and Technology through grant number SB/S3/CE/072/2014. BKB acknowledges an Inspire fellowship from the Department of Science and Technology. We acknowledge the IUSSTF Joint Center for Nanoparticle Assemblies that made it possible to have discussions with Prof. Sanat Kumar, Columbia University, USA.

Notes and references

1 W. L. Li, K. Lu and J. Y. Walz, *Intern. Mater. Rev.,* 2012, **57**, 38.
2 S. Deville, *Adv. Eng. Mater.*, 2008, **10**, 155.
3 M. C. Gutiérrez, M. L. Ferrer and F. Del Monte, *Chem. Mater.*, 2008, **20**, 634.
4 D. N. Ross, Lancet, 1962, **2**, 487.
5 T. M. Freyman, I. V. Yannas and L. J. Gibson, *Prog Mater. Sci.,* 2001, **46,** 273.
6 J. A. Talalay, *US Patent 2,432,353,* 1947.
7 S. R. Mukai, H. Nishihara, T. Yoshida, K. I. Taniguchi and H. Tamon, *Carbon,* 2005, **43**, 1563.
8 F. J. O'Brien, B. A. Harley, I. V. Yannas and L. Gibson, *Biomaterials*, 2004, **25**, 1077.
9 N. Dagalakis, J. Flink and P. J. Stasikelis, *Biomed. Mater. Res.*, 1980, **14**, 511.
10 G. Chen, T. Ushida and T. Tateishi, *Biomaterials,* 2001, **22**, 2563.
11 M. H. Ho, P. Y. Kuo, H. J. Hsieh, T. Y. Hsien, L. T. Hou, J. Y. Lai and D. M. Wang, *Biomaterials,* 2004, **25**, 129.
12 M. H Ho, D. M. Wang, C. E. Liu, C. H. Hsieh, H. C. Tseng and H. J. Hsieh, *Carbohydr. Polym.,* 2007, **67**, 124.
13 R. Ricciardi, F. Aureimma and C. De Rosa, *Macromol. Symp.*, 2005, **222**, 49.
14 W. Mahler and M. F. Bechtold, *Nature,* 1980, **285**, 27.
15 S. R. Mukai, H. Nishihara, S. Shichi and H. Tamon, *Chem. Mater.,* 2004, **16**, 4987.
16 S. R. Mukai, H. Nishihara and H. Tamon, *Chem. Commun.*, 2004, **116**, 874.
17 H. Nishihara, S. R. Mukai, Y. Fujii, T. Tago, T. Masuda, H. Tamon, *J. Mater. Chem.,* 2006, **16**, 3231.
18 H. Zhang, I. Hussain, M. Brust, M. F. Butler, S. P. Rannard and A. I. Cooper, *Nat. Mater.,* 2005, **4**, 787.
19 S. Deville, E. Saiz, R. K. Nalla and A. P. Tomsia, *Science,* 2006, **311**, 515.
20 E. Munch, M. E. Launey, D. H. Alsem, E. Saiz, A. P. Tomsia and R. O. Ritchie, *Science,* 2008, **322**, 1516.
21 F. Bouville, E. Maire, S. Meille, B. Van De Moortèle, A. J. Stevenson and S. Deville, *Nat. Mater*., 2014, **13**, 508.
22 Q. Shi, Z. An, C. K. Tsung, H. Liang, N. Zheng, C. J. Hawker and G. D. Stucky, *Adv. Mater.,* 2007, **19**, 4539.
23 C. A. L. Colard, R. A. Cave, N. Groissard, J. A. Covington and S. A. F. Bon, *Adv. Mater.,* 2009, **21**, 2894.
24 J. L. Vickery, A. J. Patil and S. Mann, *Adv. Mater.,* 2009, **21**, 2180.
25 P. Vesilind and C. Martel, *J. Environ. Eng.,* 1990, **116**, 854.
26 K. A. Jackson and B. Chalmers, *J. Appl. Phys.,* 1958, **29**, 1178.
27 D. R. Uhlmann, B. Chalmers and K. A. Jackson, *J. Appl. Phys.,* 1964, **35**, 2986.
28 J. Cisse and G. F. Bolling, *J. Crystal Growth,* 1971, **10,** 67.
29 J. S. Langer, *Rev. Modern Phys.,* 1980, **52**, 1.
30 W.W. Mullins and R. F. Sekerka, *J. Appl. Phys.,* 1964, **35**, 444.
31 M. F. Butler, *Cryst. Growth Des.*, 2001, **1**, 213.
32 S. S. L. Peppin, J. A. W. Elliot and M. G. Worster, *J. Fluid Mech.,* 2006, **554**, 147.
33 S. S. L. Peppin, J. S. Wettlaufer and M. G. Worster, *Phys. Rev. Lett.,* 2008, **100**, 238301.
34 S. Deville, E. Maire, G. Bernard-Granger, A. Lasalle, A. Bogner, C. Gauthier, J. Leloup, and C. Guizard, *Nat. Mater.,* 2009, **8,** 966.
35 S. Deville, E. Maire, A. Lasalle, A. Bogner, C. Gauthier, J. Leloup and C. Guizard, *J. Am. Ceram. Soc.,* 2010, **93**, 2507.
36 A. Lasalle, C. Guizard, E. Maire, J. Adrien and S. Deville, *Acta Mater.,* 2012, **60**, 4594.
37 S. Deville, J. Adrien, E. Maire, M. Scheel and M. Di Michiel *Acta Mater.,* 2013, **61**, 2077.
38 R. Rajamanickam, S. Kumari, D. Kumar, S. Ghosh, J. C. Kim, G. Tae, S. Sengupta and G. Kumaraswamy, *Chem. Mater.,* 2014, **26**, 5161.
39 D. Frenkel D. and B. Smit (1996), Understanding molecular simulation; Academic (London).
40 K. P. Sharma, A. K. Ganai, S. Sengupta, and G. Kumaraswamy, Chem. Mater., 2011, **23**, 1448.
41 J.P. Hoogenboom, D. Derks, P. Vergeer, and A. van Blaaderen *J. Chem. Phys*., 2002 **117**, 11320
42 M. Holgado, F. García-Santamaría, A. Blanco, M. Ibisate, A. Cintas, H. Míguez, C. J. Serna, C. Molpeceres, J. Requena, A. Mifsud, F. Meseguer, and C. López *Langmuir* 1999, **15**, 4701–4704
43 T. Vicsek and F. Family *Phys. Rev. Lett.* 1984, **52**, 1669
44 David M. Heyes and John R. Melrose *Mol. Phys*, 1989, **66**, 1057-1074
45 J. C. F. Toledano, F. Sciortino and E. Zaccarelli *Soft Matter*, 2009, **5**, 2390-2398
46 S. C. Glotzer, *J. Non-Cryst. Solids*, 2000, **274,** 242- 255
47 C. Valeriani, E. Sanz, P. N. Pusey, W. C. K. Poon, M. E. Cates and E. Zaccarelli *Soft Matter*, 2012, **8**, 4960-4970

48 E. M. Furst, C. Suzuki, M. Fermigier, A. P. Gast *Langmuir* 1998, **14**, 7334.
49 E. M. Furst , A. P. Gast *Phys. Rev. E* 2000, **62**, 6916.
50 A. L. Hiddessen, S. D. Rodgers, D. A. Weitz, and D. A. Hammer *Langmuir*, 2000, **16**, 9744.
51 S. L. Biswal, and A. P. Gast *Anal. Chem.* 2004, **76**, 6448.
52 Z. Nie, D. Fava, E. Kumacheva, S. Zou, G. C. Walker and M. Rubinstein, *Nat. Mater., 2007,* **6**, 609.
53 K. Liu, Z. Nie, N. Zhao, W. Li, M. Rubinstein and E. Kumacheva, *Science,* 2010, **329**, 197.
54 S. Sacanna, W. T. M. Irvine, P. M. Chaikin and D. J. Pine *Nature*, 2010, **464**, 575.
55 D. Li, S. Banon and S. L. Biswal *Soft Matter*, 2010, **6**, 4197.
56 Y. Wang, Y. Wang, D. R. Breed, V. N. Manoharan, L. Feng, A. D. Hollingsworth, M. Weck and D. J. Pine *Nature* 2012, **491**, 51.
57 H. R. Vutukuri; A. F. Demiroers, B. Peng, P. D. J. van Oostrum, A. Imhof and A. van Blaaderen, *Angew Chem. Intl. Ed*., 2012, **51**, 11249.
58 B. Bharti, G. H. Findenegg and O. D. Velev, *Sci. Rep.*, 2012, **2**, 1004.
59 M. B. Bannwarth, S. Utech, S. Ebert, D. A. Weitz, D.l Crespy, and K. Landfester, *ACS Nano,* 2015, **9**, 2720.
60 J.P. Hoogenboom, D.Derks, P.Vergeer, and A. van Blaaderen

Concentration of colloidal particles per ml	No. of colloidal particles in simulation box	No. of ice nuclei in simulation box	Total no. of particles in simulation box	Box dimensions (μm)
10^6	1000	5000	6000	1000.0 x 1000.0 x 1000.0
10^7	1000	500	1500	464.1 x 464.1 x 464.1
10^8	950	50	1000	215.0 x 215.0 x 215.0
10^9	995	5	1000	100.0 x 100.0 x 100.0

Table 1: Simulation system details.

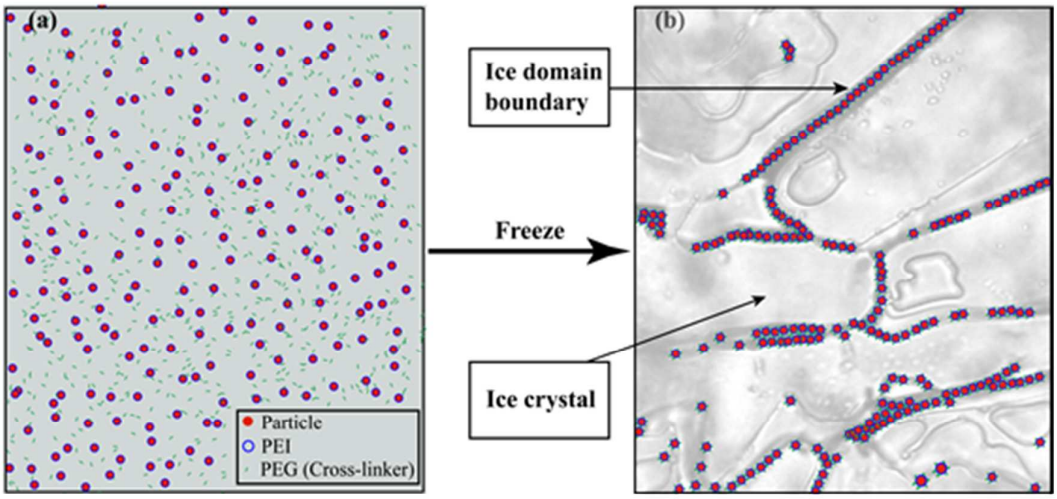

Figure 1: Schematic of the ice templating process. On freezing a dilute dispersion, latex particles (in red), polymer (PEI, in blue) and crosslinker (in green), segregate to the boundries of ice crystals and are crosslinked to form clustered aggregates.

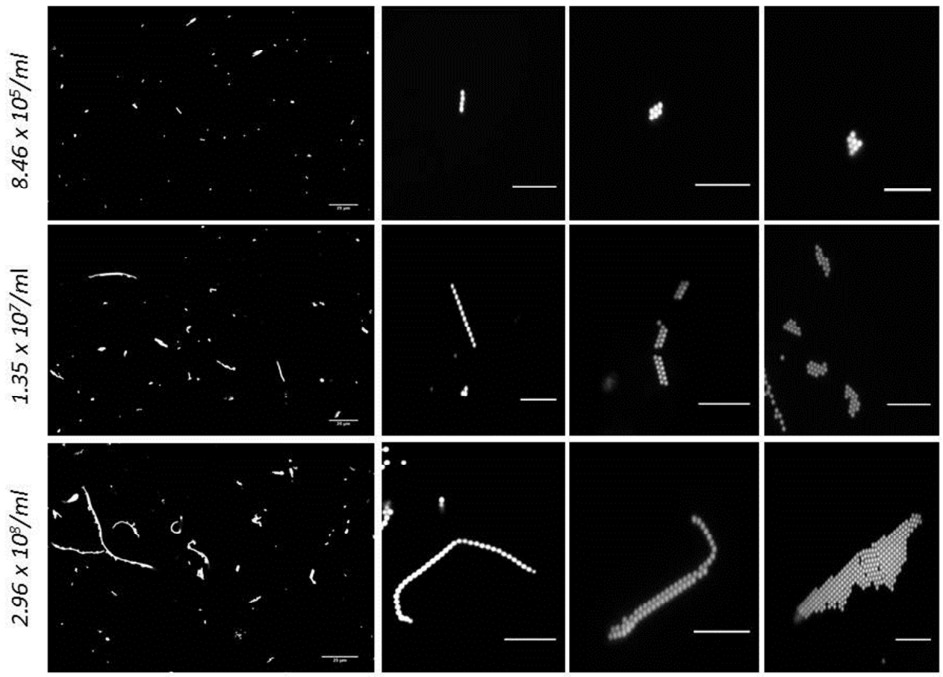

Figure 2: Microscopic images of particle aggregates from ice templating dispersions at particle concentrations of (top) 8.46 x 10^5 particles/ml; (middle) 1.35 x 10^7 particles/ml and (bottom) 2.96 x 10^8 particles/ml. The scale bar for the low magnification images on the left is 20 μm. The scale bar for the magnified images of individual clusters (block of 3 x 3 images) on the right is 10 μm.

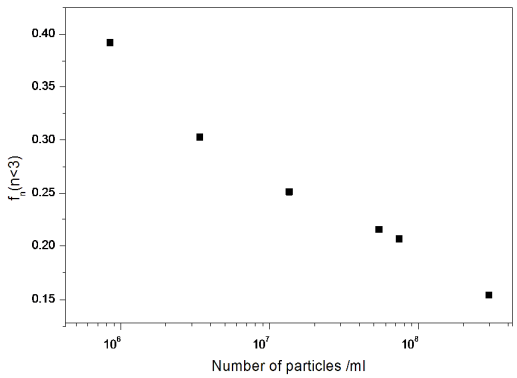

Figure 3: Fraction of particles existing as unimers or dimers after ice templating.

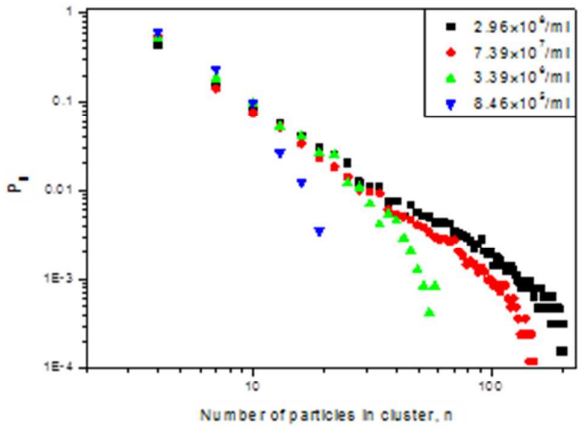

Figure 4: Cluster size distribution obtained from ice templating.

Figure

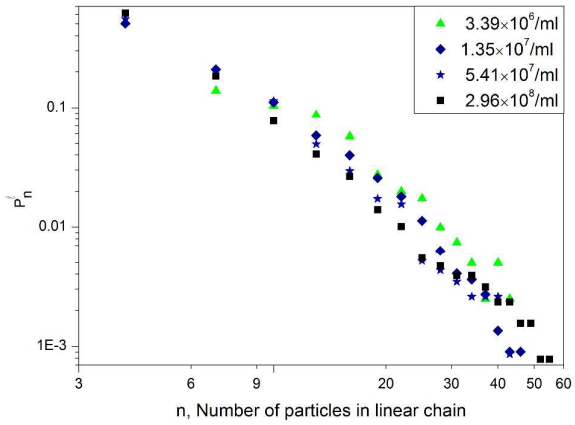

Figure 5: Size distribution of linear aggregates (colloidal chains) obtained from ice templating.

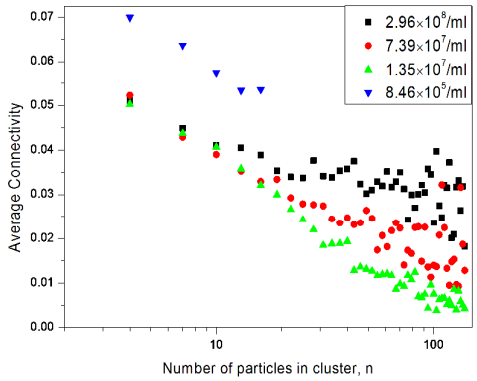

Figure 6: Variation in the average connectivity parameter with cluster size for ice templated systems at different particle concentrations.

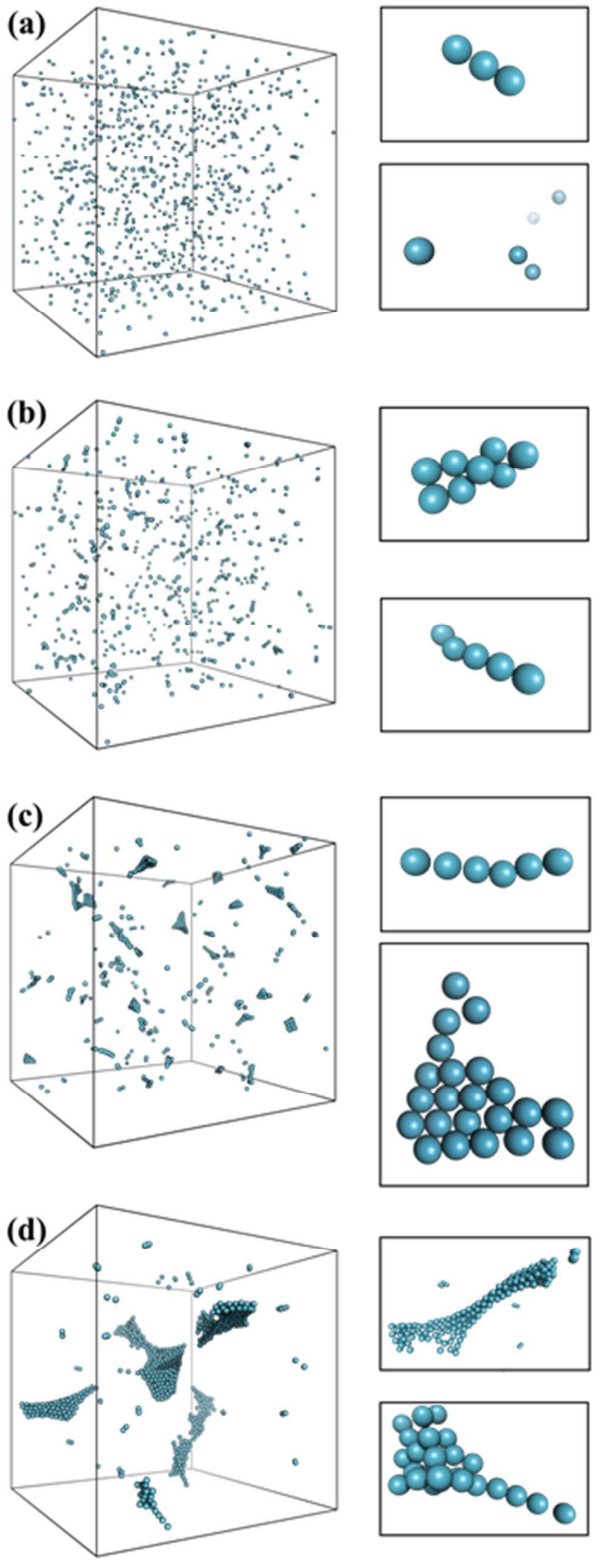

Figure 7: Snapshots of the final particle configurations from simulations of ice templated dispersions at particle concentrations of (a) 10^6 particles/ml; (b) 10^7 particles/ml; (c) 10^8 particles/ml and (d) 10^8 particles/ml. Ice crystals are not shown for ease of visualization of the particle clusters. Magnified images of some of the clusters formed are shown on the right.

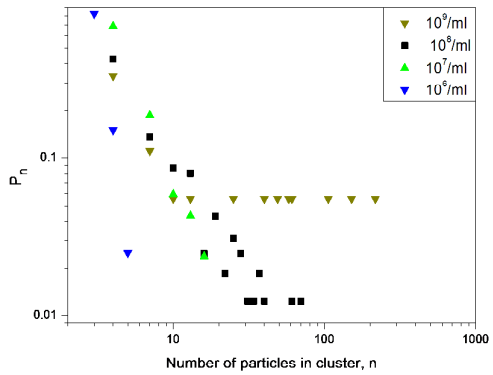

Figure 8: Cluster size distribution obtained from ice templating simulations.

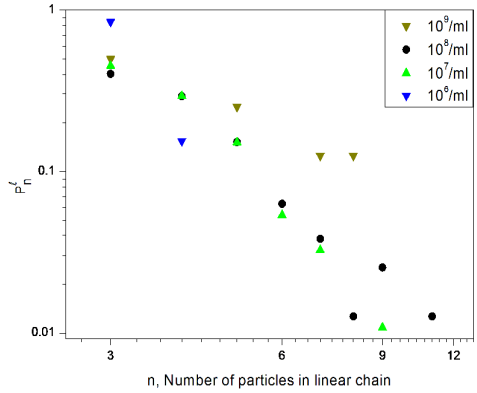

Figure 9: Size distribution of linear aggregates obtained from ice templating simulations.